Enhancement of Physical and Mechanical Properties of Oxide Dispersion-Strengthened Tungsten Heavy Alloys

WALID MOHAMED RASHAD DAOUSH, AYMAN HAMADA ABDELHADY ELSAYED, OMAYMA ABDEL GAWAD EL KADY, MOHAMED ABDALLAH SAYED, and OSAMA MONIER DAWOOD

Oxide dispersion-strengthened (ODS) tungsten heavy alloys are well known for their excellent mechanical properties which make them useful for a wide range of high-temperature applications. In this investigation, microstructural, magnetic, and mechanical properties of W-5 wt pct Ni alloys reinforced with 2 wt pct Y_2O_3, ZrO_2 or TiO_2 particles were investigated. Cold-pressed samples were sintered under vacuum at 1773 K (1500 °C) for 1 hour. The results show that, among three kinds of oxides, Y_2O_3 is the most efficient oxide to consolidate W powder by sintering. W-Ni-Y_2O_3 alloys form relatively uniform interconnected structure and also show higher density and compressive strength than those of W-Ni-ZrO_2 and W-Ni-TiO_2. On the other hand, W-Ni-TiO_2 and W-Ni-ZrO_2 alloys have non-homogeneous microstructure due to the formation of Ni globules in some areas in the matrix and almost nickel-free zones in other areas causing the appearance of pores. The Vickers hardness values for W-Ni-TiO_2 alloys are slightly higher than those of W-Ni-ZrO_2 and Ni-W-Y_2O_3 due to the smaller particle size of TiO_2 than the other oxides. At room temperature, the investigated alloys have very weak magnetic properties. This is due to the combination of the ferromagnetic nickel metal binder with the non-magnetic tungsten forming the weak magnetic W-Ni solid solution. Moreover, the measured (mass) magnetizations had small values of the power of 10^{-3} emu/g. Additionally, the values of coercivity (H_C) and remanence (M_r) for the W-Ni-TiO_2 alloy were higher than that of the W-Ni-Y_2O_3 and W-Ni-ZrO_2 alloys due to the particle size effect of TiO_2 nanoparticles.

DOI: 10.1007/s11661-016-3360-7

I. INTRODUCTION

TUNGSTEN (W) and its alloys are some of the most important materials for high-temperature applications. Among other metals, it has highest melting point, lowest vapor pressure and thermal expansion, and high thermal and electrical conductivities. Unfortunately, pure tungsten and tungsten-based materials exhibit low ductility (deformability) and low fracture toughness at all temperatures along with a high ductile-to-brittle transition temperature (DBTT) which ranges from 573 K to 1273 K (300 °C to 1000 °C).[1–5]

Tungsten heavy alloys (WHAs) are metal–metal composites consisting of nearly pure spherical tungsten particles embedded in a Ni-Fe-W, Ni-Co-W, or Ni-Cu-W ductile matrix.[6–14] Due to their high density and high strength associated with the bcc tungsten phase, and high ductility attributed to the fcc matrix, these alloys are used in applications such as kinetic energy penetrators, radiation shielding, counter balances, vibration damping devices, and other military and civil applications.[6,12,15–18]

A typical tungsten heavy alloy (WHA) contains 80 to 98 wt pct tungsten. The balance is generally a mixture of relatively low melting transition elements, such as nickel, iron, copper, and cobalt.[19–21] These alloys are traditionally made by powder metallurgy techniques involving liquid-phase sintering which helps achieve maximum densification. The elemental powders are mixed in the required ratios by weight, blended in mixers or ball mills, isostatically compressed and then sintered at a temperature between 1723 K and 1773 K (1450 °C and 1500 °C), which is enough to melt the alloying metals but not tungsten (which melts at 3723 K (3450 °C). Quenching is then employed to curb the formation of intermetallic compounds.[10] Some deformation strengthening processes, such as hydrostatic extrusion and swaging, are used to improve the tensile strength of

WALID MOHAMED RASHAD DAOUSH, Associate Professor and Department Head, is with the Department of Production Technology, Faculty of Industrial Education, Helwan University, 30 El Sawah Street, Cairo 11511-11668, Egypt. Contact e-mail: waliddaoush@techedu.helwan.edu.eg AYMAN HAMADA ABDELHADY ELSAYED, Researcher, and OMAYMA ABDEL GAWAD EL KADY, Research Assistant Professor, are with the Powder Technology Laboratory, Central Metallurgical R&D Institute (CMRDI), P.O. Box 87 Helwan, Cairo 11421, Egypt. MOHAMED ABDALLAH SAYED, Lecturer, and OSAMA MONIER DAWOOD, Professor, are with the Department of Mechanical Engineering, Faculty of Engineering, Helwan University, 11511-11668 Cairo, Egypt.

Manuscript submitted July 19, 2015.
Article published online February 8, 2016

the alloy, but the mechanical properties improvement is usually limited due to the coarse W grain microstructure fabricated by the traditional powder metallurgy process.[10,13,22]

The interest in WHA can be traced to the late 1950s and early 1960s.[12,23] Since then, a vast body of work has been generated, detailing the influence of alloying, processing, and temperature upon alloy behavior. During the last two decades, the research of tungsten heavy alloys has concentrated on strengthening methods, which is especially important in military applications.

The aim of alloying tungsten is to improve its chemical, physical, and mechanical properties at both ambient conditions and elevated temperatures. Beyond that, it is possible to combine the useful properties of tungsten with those of the alloying additives.[24] Ni can improve the properties of tungsten by its role during sintering. When the solid bonds are cut, particle rearrangement and pore filling occur, resulting in rapid densification of the compact and formation of W-Ni solid solution. Moreover, the effect of nickel on the recrystallization of tungsten has been reported by several authors. Nickel has a pronounced effect on tungsten by lowering the recrystallization temperature by several hundred degrees.[13] On the other hand, the addition of small amounts of finely dispersed oxides (mainly rare earth metals oxides) to tungsten and its alloys (oxide dispersion-strengthened alloys; ODS), for increasing their high-temperature strength, is a common practice in physical metallurgy. Oxide dispersion-strengthened (ODS) tungsten alloy is one of the most promising materials for high-temperature applications due to their high strength at elevated temperature and good oxidation resistance. Recrystallization is the factor which deteriorates high temperature strength and creep resistance of tungsten and limits its deployment in extremely high-temperature applications. These problems can be overcome by dispersion strengthening and precipitation hardening, as in the case of W-ThO_2.[24,25] However, the radioactive nature of thorium has turned development efforts toward tungsten alloys strengthened by other metal oxides like La_2O_3,Y_2O_3, HfO_2, ZrO_2, CeO_2.[26–29] Dispersed oxide particles inhibit recrystallization and grain growth and improve the high temperature strength and creep resistance by hindering grain boundary sliding.[26–29]

In this paper, the aim is to improve tungsten heavy alloys by different dispersed oxides. The effects of 2 wt pct Y_2O_3, ZrO_2, or TiO_2 particles on the consolidation behavior, microstructure, and magnetic and mechanical properties of W-5 wt pct Ni alloys were investigated.

II. EXPERIMENTAL WORK

Tungsten powder (99.95 pct, 0.5 to 3 μm) purchased from Buffalo Tungsten, INC., Y_2O_3 (99.995 pct, <1 μm), ZrO_2 (99.9 pct, 300 to 700 nm), TiO_2 (99 pct, 200 nm) powders purchased from Inframat Advanced Materials, and Ni powder (99.7 pct, 1 to 2 μm) purchased from Jin Sheng International Industrial Ltd were used in this study. The as-received powders were investigated by scanning electron microscope to determine the particle size and shape. WHAs containing 93 wt pct W, 2 wt pct oxide, and 5 wt pct Ni were prepared by powder metallurgy technique. The elemental powders of W, Ni, and Y_2O_3, ZrO_2, or TiO_2 were ball milled together for 24 hours for homogenization and particle size reduction to improve sintering behavior. Dry ball milling process was performed to prepare 200 grams from each composition of the investigated samples by means of home-made high-strain ball mill using hard steels balls of 6 mm diameter in a container made from H13-hardened tool steel with balls to powder mass ratio of 10:1 and milling speed of 80 rpm. Following the milling process, the mixtures were then pressed at room temperature under the compaction pressure of 100 MPa. The green compacts were sintered at the temperature of 1773 K (1500 °C) in a vacuum furnace for 1 hour using the heating rate of 10 °C/min. Extensive metallographic investigations were conducted to evaluate the microstructure of the fabricated WHAs using scanning electron microscopy (model JEOL-JSN-5410). The phase identifications and the chemical compositions of the investigated WHAs were performed using XRD (model X, Pert PRO analytical with Cu k_α radiation, $\lambda = 0.15406$). The density of the sintered materials was measured by Archimedes principle using water as the floating liquid. The magnetic properties of samples were measured using vibrating sample magnetometer (model DEAS/FDD-2) in which the samples were vibrated at a constant frequency between a set of sense coils. As the magnetic field is varied through a specified range, the magnetic moment of the sample is measured by the sense coils with a lock-in amplifier. The dependency between the magnetization and magnetic field (hysteresis loop) for the prepared WHA samples was measured. The magnetization values were expressed using the magnetic moment per gram (emu/g). The measured properties included magnetic saturation (M_s), coercivity (H_c), and remnant magnetization (retentivity) (M_r).

The hardness values of the investigated materials were measured as the average of five readings along the cross-section surface of the specimens using Vickers hardness test (model Indentec 5030 SKG) at a load of 30 Kg for 15 seconds. The compressive strength was also measured on cylindrical test specimens. The specimen area was 28.2743 mm^2 and the strain rate was 5 mm/min. The maximum compression load for each specimen was recorded, and the compressive strength was determined.

III. RESULTS AND DISCUSSION

A. *Microstructure and Phase Analysis*

The as-received powders were characterized for their size, size distribution, and morphology. The SEM micrographs of the used powders which are W, Y_2O_3, ZrO_2, TiO_2, and Ni are shown in Figures 1(a) through (e), respectively. The W powder particles are equiaxed with a size range of approximately 0.5 to 4 μm. Y_2O_3

powder has a flake shape with a size <1 μm. ZrO_2 powder has a rounded shape with some agglomerations. The particle size of ZrO_2 powder ranges between 0.3 and 0.7 μm. TiO_2 powders is very fine with equiaxed grains ranging from 100 to 200 nm. Also the micrographs showed that Nickel powder has spherical particle shape with 0.5 to 2 μm particle size. From these results, one can notice that some powders have spherical shapes and others have irregular shapes with some variation in particles sizes. This results in good packing, fluidity, and compressibility of powders and eventually improves the properties of sintered samples.

Figures 2 (a), (b), and (c) show the SEM micrographs of W-Ni-Y_2O_3, W-Ni-TiO_2, and W-Ni-ZrO_2 samples, respectively. It was found that the rare earth oxide particles are homogeneously dispersed in the matrix. These oxide particles inhibit the formation of the metal oxide in the matrix and decrease the grain growth. Also, the oxide particles increase the densifications and decrease the porosity content by capturing the oxygen in the matrix.

The microstructure of W-Ni-Y_2O_3 in Figure 2(a) indicates the formation of nickel globules and almost nickel-free zones due to the appearance of pores. It can be also noticed that the oxide particles have been preferentially located at the Ni globules, which could be confirmed by the EDS mapping, as shown in Figure 3. This is due to the liquid-phase sintering of the compacted powders.

The formation of the globules increased in case of W-Ni-TiO_2 and W-Ni-ZrO_2 as shown in Figures 2(b) and (c), respectively. These globules are appearing clearly (see Figure 3) in the mapping micrographs of W-Ni-TiO_2. Figure 2(c) shows coarser microstructure of W-Ni-ZrO_2 (mean particle size of W $\approx$ 19.8 μm) than W-Ni-Y_2O_3 (mean particle size of W $\approx$ 14.7 μm) and W-Ni-TiO_2 (mean particle size of W $\approx$ 14.1 μm) (Figures 2(a) and (b)). The reason on one hand is the addition of Y_2O_3 particles which leads to grain refinement as mentioned in previous work.[4,18,22] It was reported that Y_2O_3 is an oxide which enhances the sinterability of W powders. It means the particle acts as an activator during sintering and the paths through which the atoms move are increased and thereby the sinterability of W powder may be promoted. On the other hand, the fine microstructure of W-Ni-TiO_2 is due to the presence of fine initial particle of TiO_2 (~200 nm) which helps in refining microstructure. The consolidation process of W-rare metal oxide occurs usually through either of two processes, solid-state or local liquid sintering. The former is the consolidation of W powder which can be supported by the presence of W polyhedral grains. The latter is the eutectic reaction between W and the oxide phases which is formed at certain temperatures near 1773 K (1500 °C) and at certain composition. This means the melting temperature of W is decreased by adding the metal oxide content. Above that temperature, W atoms can move

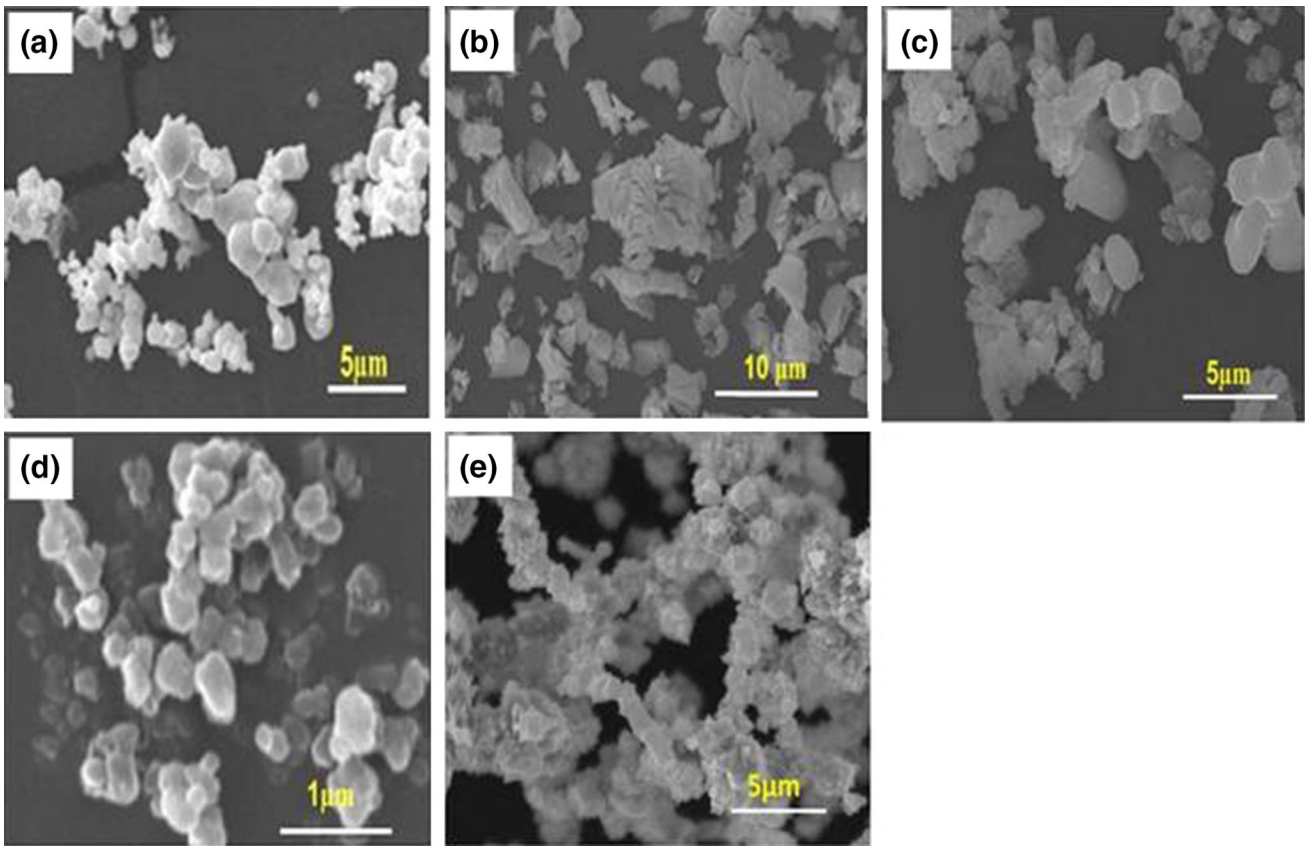

Fig. 1—SEM micrographs of the as-received powders: (*a*) W, (*b*) Y_2O_3, (*c*) ZrO_2, (*d*) TiO_2, and (*e*) Ni.

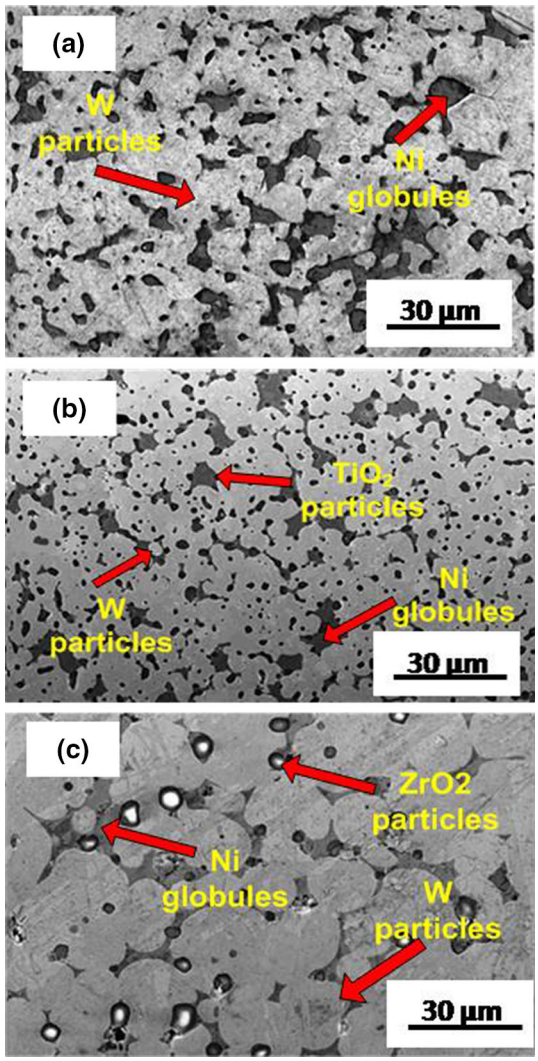

Fig. 2—SEM micrographs of the produced WHAs: (*a*) W-Ni-Y_2O_3, (*b*) W-Ni-TiO_2, and (*c*) W-Ni-ZrO_2.

through the oxide particles as well as W grain boundaries. In addition, all oxides play a role in inhibiting the W grain coarsening by hindering the grain growth. However, there is no evidence to support the phenomenon in this work. It was reported that the sintered W-Y_2O_3 composite is composed of W and Y_2O_3 phases only and there is not any direct observation that eutectic reaction between the two phases occurs.[30–32]

The X-ray diffraction patterns of the fabricated WHAs revealed the presence of peaks which belong to bcc-structured tungsten phase, as shown in Figure 4. However, three relatively weak peaks which correspond to Ni–W solid solution phase were also found in these diffraction patterns.

B. *Physical Properties of WHAs*

The density of WHAs is one of the most important properties as it affects both physical and mechanical properties of the composite. Figure 5 shows the relative sintered densities of the investigated specimens. The densities were measured by Archimedes method and the reliability of measurements was ±0.001 g.

It is obvious that the relative sintered density of W-Ni-Y_2O_3 sample is higher than that of W-Ni-ZrO_2 and W-Ni-TiO_2. This may be attributed to the presence of Y_2O_3 particles which improves the densification of W powders. This is in agreement with the previous work on the sintering of WHAs which showed that the addition of only 0.02 wt pct Y_2O_3 increases the relative density of the material by about 1 pct.[4,23] This is in agreement with the previous work on the sintering of WHAs[4] which showed that the addition of only 0.02 wt pct Y_2O_3 increases the relative density of the sintered materials by about 1 pct and the relative sintering density reach 99.3 pct.[4,23]

The lower densities of W-Ni-ZrO_2 and W-Ni-TiO_2 may be attributed to the presence of porosity, which in turn is due to micro-swelling or micro-bubbles which easily formed on the surface of the sintered samples without Y_2O_3 addition. The reason for those bubbles is related to impurities and oxygen contamination during milling process. It is suggested also that the source of such gases could be the result of incipient melting of the new oxides during the sintering. The entrapped gases expand by heating during sintering. During the cooling stage, after the sintering cycle, the high circumferential pressure imposed by the contracting metal grains may have resulted in blowing up of gas bubbles. However, Y_2O_3 is preferential to inhibit oxide formation which prevents effectively defects and porosity formation.[22,24,33,34]

Tungsten heavy alloys are increasingly used worldwide as radiation shields for specific applications, so measurements of the magnetic properties are important. Non-magnetic materials have to be used whenever the magnetic fields cannot be perturbed in radiation equipment or when shielding is positioned near electrical sensors.[35] In this investigation, the magnetic properties of WHA composites: W-Ni-Y_2O_3, W-Ni-TiO_2, and W-Ni-ZrO_2 were examined. The relation between the magnetization (M) and the magnetic field (H) (the M-H hysteresis loop) was measured at room temperature. The measured hysteresis loops are presented in Figure 6. The values of magnetization (M_s), coercivity (H_c), permeability (μ_r), and remnant magnetization (M_r) are listed in Table I. The shape of the obtained loops, as well as the small values of magnetization, indicates that the investigated materials have weak magnetic behavior at room temperature. The samples are also difficult to saturate under the examined field. However, the pure nickel sample was saturated under the examined field of 5 kOe (see Figure 6(a)). This is in agreement with previous work on magnetic properties of tungsten alloys.[35]

It was observed from the results that, at room temperature and under the applied field of 5 kOe, the measured magnetization values were equal to 8.593×10^{-3}, 8.345×10^{-3}, and 8.232×10^{-3} emu/g, for the investigated W-Ni-TiO_2, W-Ni-Y_2O_3, and W-Ni-ZrO_2 alloys, respectively. For comparison, the magnetizations for Fe, Co, and Ni are equal to 218, 161, and 54.8 emu/g, respectively.[36] The saturation magnetization (M_S) is an intrinsic property independent on the grain size and microstructure but is affected mainly by

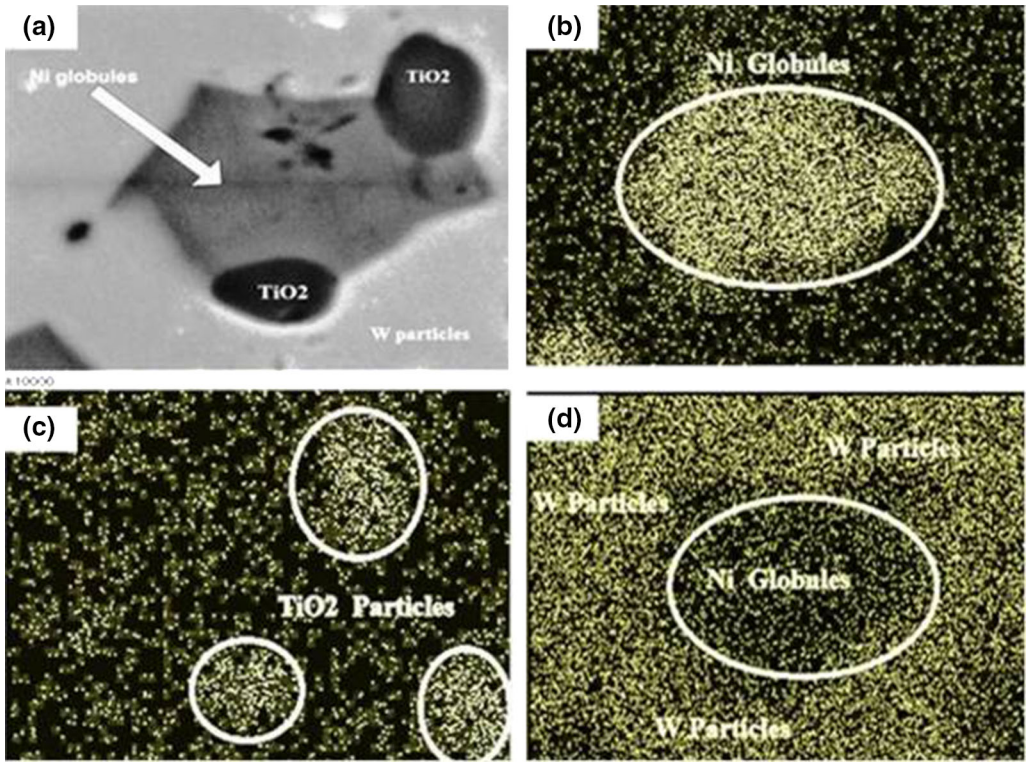

Fig. 3—SEM Mapping of the investigated Ni-W-TiO_2 WHAs: (*a*) W-Ni-TiO_2, (*b*) Ni globules, (*c*) TiO_2 particles, and (*d*) W particles.

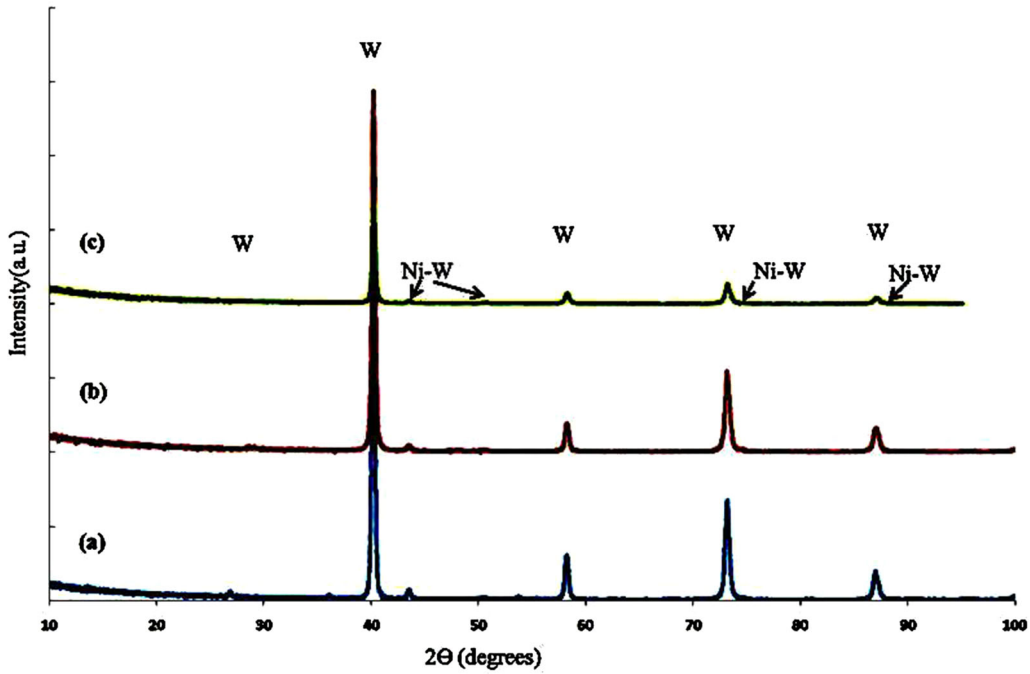

Fig. 4—XRD patterns of the produced WHA-sintered materials at 1500 °C under vacuum: (*a*) W-Ni-TiO_2, (*b*) W-Ni-Y_2O_3 and (*c*) W-Ni-ZrO_2.

the composition of the alloy.[37] Magnetic behaviors of the obtained WHAs were mainly dependent on the contribution of the magnetic moments of the ferromagnetic nickel content. The saturation magnetization (M_S) of the investigated pure nickel is 51.15 emu/gm as shown in Figure 6(a). This value is decreased to less than unity in the case of investigated WHAs (Figures 6(c) through (e)). This is due to the formation of the solid solution between the ferromagnetic nickel metal and the non-magnetic tungsten metal which is producing a very weak magnetic Ni-W solid solution as observed in the XRD diffraction patterns (see Figure 4).

A similar trend has been reported for other binary alloys containing a non-magnetic element in solid solution, *e.g.*, Ni-Cu[35] or Fe-Al[38]. In addition, the dilution mechanism of the magnetic constituent (nickel metal) in the whole WHAs governs the overall magnetization behavior, which is in agreement with both the work on W-Co alloys[39] and our previous work on W-Co alloys and (W,Ti)C-Ni-sintered materials[39] and,[40] respectively.

Conversely, coercivity, H_C, and remanence, M_r, can be regarded as extrinsic properties dependent both on grain size and microstructure, as well as on grain shape, texture, and internal stresses.[36,41] The results also showed that the values of coercivity (H_C) and remanence (M_r) of W-Ni-TiO_2 are higher than that of W-Ni-Y_2O_3 and W-Ni-ZrO_2 alloys. This is due to the particle size effect of the added TiO_2 particles which have a particle size in the nanoscale (100 to 200 nm). The magnetic domains of the added nano-TiO_2 particles can rotate and rearrange under the applied field (increase the coercivity value) but the used Y_2O_3 and ZrO_2 have larger particle size which cannot affect the applied field (decreasing the coercivity value).

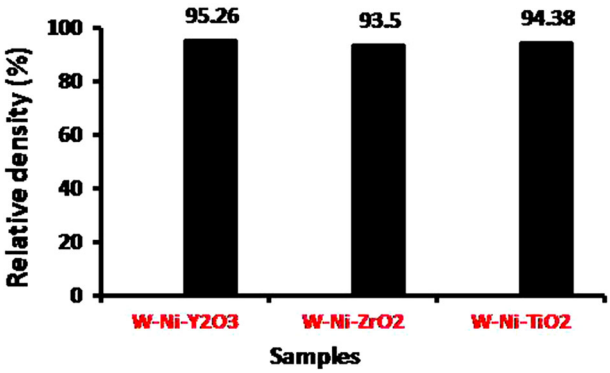

Fig. 5—Relative densities of the produced WHA-sintered materials at 1773 K (1500 °C) under vacuum.

C. *Mechanical Properties*

The Vickers hardness values of the investigated samples are shown in Figure 7. The hardness values of investigated samples given in the figure are the average of five readings, which have shown small variation within each sample. It can be seen that the hardness of the W-Ni-TiO_2 alloy is higher than those of the W-Ni-ZrO_2 and W-Ni-Y_2O_3 alloys. These results can be attributed to the finer microstructure in case of TiO_2 addition, which always has the strongest effect on hardness. It might also be attributed to the effect of nickel distribution on the matrix and porosity content. As the nickel particles and pores decrease in a certain area of tungsten matrix, the hardness increases. The increase in hardness due to the lower Ni content in some areas is due to the higher hardness value of tungsten phase. Hardness values of all investigated samples are

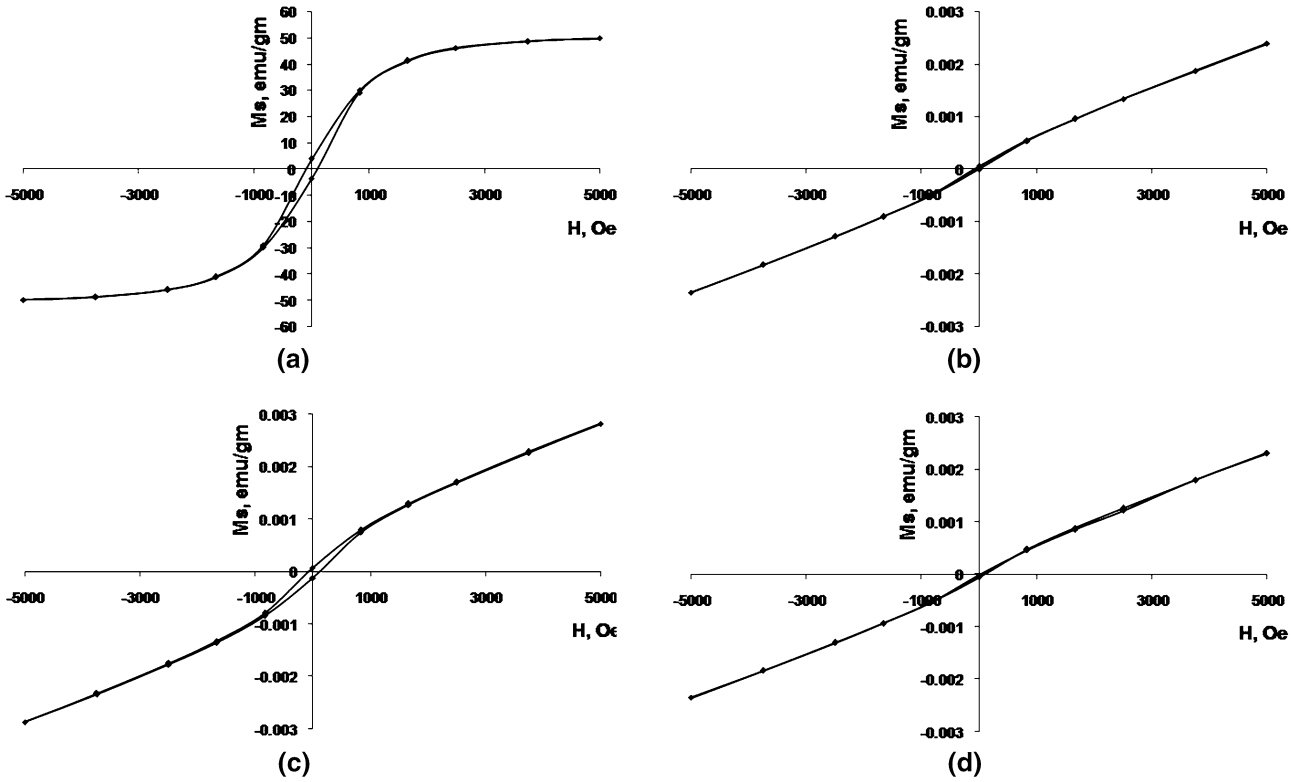

Fig. 6—M-H Magnetization curves (Hysteresis loops) of the investigated materials: (*a*) Ni metal, (*b*) W-Ni-Y_2O_3, (*c*) W-Ni-TiO_2, and (*d*) W-Ni-ZrO_2.

Table I. Magnetic Properties of the Investigated Materials

Magnetic Properties			
M_r (emu/g)	H_c (Oe)	M_s (emu/g)	Investigated Samples
3.771	96.059	51.152	Ni metal
9.76×10^{-5}	94.092	8.593×10^{-3}	W-Ni-TiO_2
3.40×10^{-5}	52.460	8.345×10^{-3}	W-Ni-Y_2O_3
2.21×10^{-5}	32.973	8.232×10^{-3}	W-Ni-ZrO_2

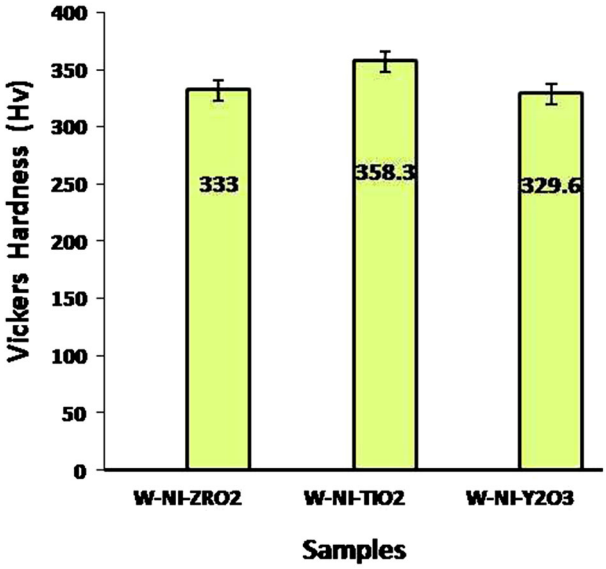

Fig. 7—Hardness values of the produced WHA-sintered materials at 1773 K (1500 °C) under vacuum.

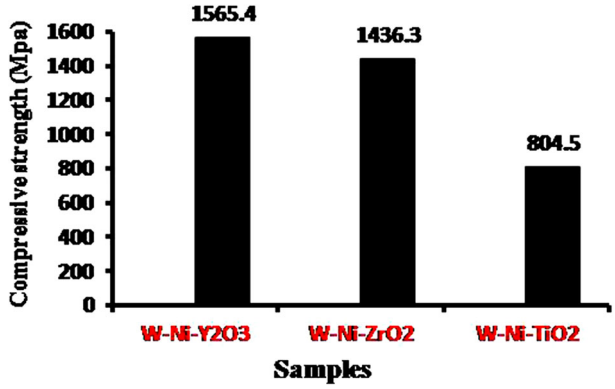

Fig. 8—Compressive strength values of the produced WHA-sintered materials at 1773 K (1500 °C) under vacuum.

relatively lower than those reported in previous work. This is because the hardness is reduced when the sintering temperature is raised to more than 1350 °C, due to the rapid increase in the tungsten grain size.[42]

The compressive strength was determined using cylindrical specimens. The compressive strength results for the investigated WHAs are shown in Figure 8. It is evident that the compressive strength of the W-Ni-Y_2O_3 composites was higher than that of W-Ni-ZrO_2 and W-Ni-TiO_2. This may be attributed to the presence of Y_2O_3 particles, as the addition of Y_2O_3 particles to a W matrix leads to grain refinement and improve strength at room and high temperature.[4,18,22] The compressive strength increased with increasing density and decreasing porosity. Further investigation of low compressive strength value for TiO_2-added specimen, the fracture surfaces, examined by a field emission scanning electron microscope, of the compression test specimens are shown in Figure 9. Both specimens with Y_2O_3 and ZrO_2 additions have shown dimpled pattern fracture appearances with no clear sign of particle surface separation. On the other hand, the specimen with TiO_2 addition has revealed the presence of a near-surface region that is almost free from Ni that might have been formed due to excessive local melting of Ni, as shown in Figures 9(c) and (d). The bonds between W particles have consequently been dramatically reduced, forming a void-like fracture initiation site (the dark area in the figure). At that region, the W particles appear detached from each other. On the other hand, other positions on the fracture surface (bright area) have shown a normal fracture appearance with a dimpled pattern.[43]

IV. CONCLUSION

This study investigated the processing of oxide dispersion-strengthened (ODS) tungsten heavy alloys by powder metallurgy route through liquid-phase sintering under vacuum at 1773 K (1500 °C). The influence of the oxide types on the physical and mechanical properties of the WHAs can be understood by investigating the corresponding microstructures. W-Ni-TiO_2 has finer microstructure and smaller grains size than W-Ni-ZrO_2 and W-Ni-Y_2O_3 due to the smaller particle size of the reinforced TiO_2 particles than the other oxides particles of ZrO_2 and Y_2O_3. The effect of dispersing oxides on the densification of W composite is quite different according to the kinds of oxides. However, the W-Ni-Y_2O_3 alloy achieved higher densification and lower porosity than that of W-Ni-ZrO_2 and W-Ni-TiO_2. The Magnetic properties which were obtained by measuring the M-H hysteresis loops of the investigated WHAs show that the produced three WHAs have very weak magnetic properties due to the formation of the weak magnetic W-Ni solid solution in the matrix phase. The measured magnetizations were extremely have small values to the power of 10^{-3} emu/g for the produced three WHAs samples. The values of coercivity (H_C) and remanence (M_r) of W-Ni-TiO_2 are

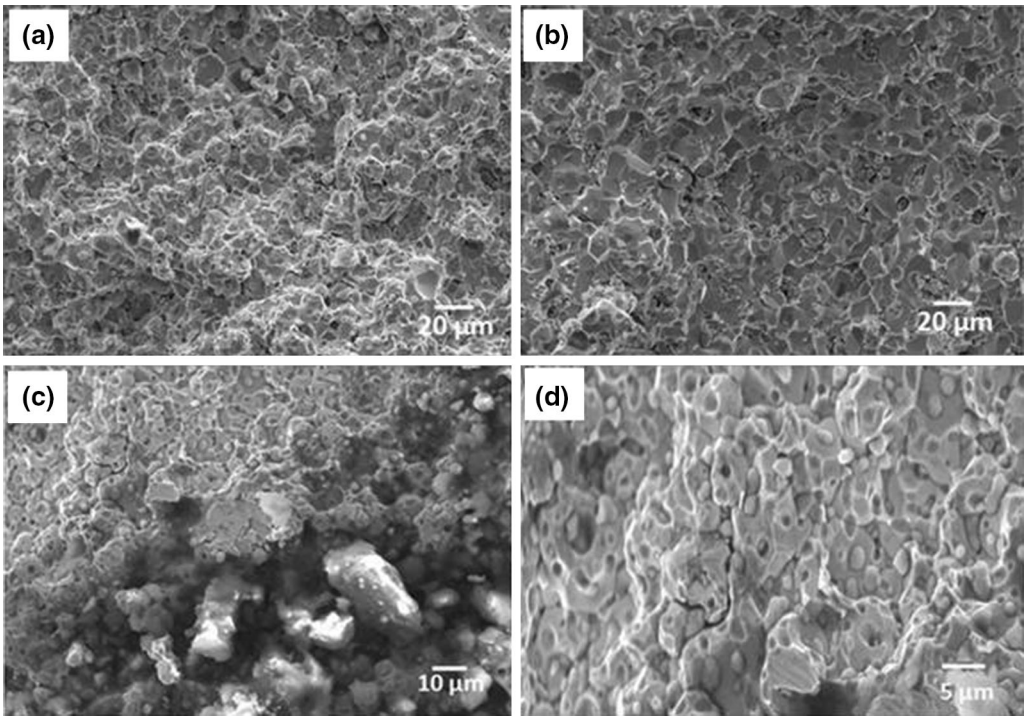

Fig. 9—Fractography of the produced W-Ni-Y_2O_3 (*a*), W-Ni-ZrO_2 (*b*), and W-Ni-TiO_2 (*c* and *d*).

higher than those of W-Ni-Y_2O_3 and W-Ni-ZrO_2 due to the particle size effect of the reinforced nanosized TiO_2 particles. The Vickers hardness results show that the W-Ni-TiO_2 alloy achieved higher values than those of the W-Ni-ZrO_2 and W-Ni-Y_2O_3 alloys. High compressive strength is obtained from W-Ni-Y_2O_3 alloy and the value increased by increasing the bulk density. The produced sintered materials are expected to offer interesting prospective properties for WHA applications.

ACKNOWLEDGMENT

The authors are grateful to the late Professor of Powder Technology, Professor Sayed Farag Moustafa, at the Central Metallurgical Research and Development Institute, who had suggested the line of this work, and pray to God to let his soul rest in peace.

REFERENCES

1. Y. Kim, M.H. Hong, S.H. Lee, E.P. Kim, S. Lee, and J.W. Noh: *Met. Mater. Int.*, 2006, vol. 12 (3), pp. 245–48.
2. C.H. Henager, R.J. Kurtz, T.J. Roosendaal, and B.A. Borlaug: *Fusion React. Mater. Program*, 2013, vol. 55, pp. 29–39.
3. L. Velevaa, Z. Oksiuta, U. Vogtb, and N. Baluca: *Fusion Eng. Des.*, 2009, vol. 84, pp. 1920–24.
4. L. Veleva: Contribution to the Production and Characterization of W-Y, W-Y_2O_3 and W-TiC Materials for Fusion Reactors, Doctor of Philosophy, 2011, pp. 1–164.
5. W. Liu, Y. Ma, and J. Zhang: *Int. J. Refract. Met. Hard Mater.*, 2012, vol. 35, pp. 138–42.
6. S.H. Islam, F. Akhtar, S.J. Askari, M.T. Jokhio, and X. Qu: *NED Univ. J. Res.*, 2009, vol VI, no. 1.
7. A. Upadhyaya, S.K. Tiwari, and P. Mishra: *Scr. Mater.*, 2007, vol. 56, pp. 5–8.
8. N.K. Caliskan, N. Durlu, and S. Bor: *Int. J. Refract. Met. Hard Mater.*, 2013, vol. 36, pp. 260–64.
9. K.H. Lee, S.I. Cha, H.J. Ryu, and S.H. Hong: *Mater. Sci. Eng. A*, 2007, vols. 452–453, pp. 55–60.
10. A. Ogundipe, B. Greenberg, W. Braida, C. Christodoulatos, and D. Dermatas: *Corr. Sci.*, 2006, vol. 48, pp. 3281–97.
11. F.D.S. Marquis, A. Mahajan, and A.G. Mamalis: *J. Mater. Process. Technol.*, 2005, vol. 161, pp. 113–20.
12. K.R. Tarcza: The Dynamic Failure Behavior of Tungsten Heavy Alloys Subjected To Transverse Loads, Doctor of Philosophy, 2004, pp. 1–186.
13. Y. Wu, R.M. German, B. Marx, R. Bollina, and M. Bell: *Mater. Sci. Eng. A*, 2003, vol. 344, pp. 158–67.
14. E. Fortuna, W. Zielinski, K. Sikorski, and K.J. Kurzydlowski: *Mater. Chem. Phys.*, 2003, vol. 81, pp. 469–71.
15. S.H. Hong and H.J. Ryu: *Mater. Sci. Eng. A*, 2003, vol. 344, pp. 253–60.
16. S.H. Hong, H.J. Ryu, and W.H. Baek: *Mater. Sci. Eng. A*, 2002, vol. 333, pp. 187–92.
17. R. Gero, L. Borukhin, and I. Pikus: *Mater. Sci. Eng. A*, 2001, vol. 302, pp. 162–67.
18. HJ Ryu and SH Hong: *Mater. Sci. Eng. A*, 2003, vol. 363, pp. 179–84.
19. A Upadhyaya: *Mater. Chem. Phys.*, 2001, vol. 67, pp. 101–10.
20. D.J. Williams, S. Clyens, and W. Johnson: *Pow. Metall.*, 1980, vol. 2, pp. 92–94.
21. J. Lezanski and W. Rutkowski: *Metall. Int.*, 1987, vol. 19, pp. 29–31.
22. F. Jing-lian, L. Tao, C. Hui-chao, and W. Deng-long: *J. Mater. Process. Technol.*, 2008, vol. 208, pp. 463–69.
23. K.H. Lin, C.S. Hsu, and S.T. Lin: *Int. J. Refract. Met. Hard Mater.*, 2003, vol. 21, pp. 193–203.
24. J.W. Pugh: *Metall. Trans.*, 1973, vol. 4 (2), pp. 533–38.
25. P.K. Wright: *Metall. Trans. A*, 1978, vol. 9A, pp. 955–63.
26. J.W. Davis, V.R. Barabash, A. Makhankov, L. Plochl, and K.T. Slattery: *J. Nucl. Mater.*, 1998, vols. 258–263, pp. 308–12.

27. M. Mabuchi, K. Okamoto, N. Saito, M. Nakanishi, Y. Yamada, and T. Igarashi: *Mater. Sci. Eng. A*, 1996, vol. 214, pp. 174–76.
28. M. Mabuchi, K. Okamoto, N. Saito, T. Asahina, and T. Igarashi: *Mater. Sci. Eng. A*, 1997, vol. 237, pp. 241–49.
29. H.J. Ryu and S.H. Hong: *Mater. Sci. Eng. A*, 2003, vol. 363, pp. 179–84.
30. Y. Itoh and Y. Ishiwata: *JSME Int. J Ser.*, 1996, vol. A39, pp. 429–35.
31. Y. Kim, M.-H. Hong, S.H. Lee, E.-P. Kim, S. Lee, and J.-W. Noh: *Met. Mater. Int.*, 2006, vol. 12, pp. 245–51.
32. M-N Avettand-Fenoel, R Taillard, and J Dhers: *Int. J. Refract. Met. Hard. Mater.*, 2003, vol. 21, pp. 205–11.
33. E. Lassner and W.D. Schubert: *Tungsten Properties Chemistry Technology of the Element, Alloys, and Chemical Compounds*, Kluwer Academic, New York, 1999.
34. A. Upadhyaya: *Mater. Chem. Phys.*, 2001, vol. 67, pp. 101–10.
35. J.J. Bucki, E. Fortuna-Zaleśna, M. Kowalczyk, and Z. Ludyński: *Kompozyty*, 2011, vol. 11, pp. 268–73.
36. N. Tsyntsarua, H. Cesiulis, E. Pellicer, J.P. Celis, and J. Sorte: *Electrochim. Acta*, 2013, vol. 104, pp. 94–103.
37. J. Nogués, E. Apinaniz, J. Sort, M. Amboage, M. d'Astuto, O. Mathon, R. Puz-niak, I. Fita, J. S. Garitaonandia, S. Surinach, J. S. Munoz, M. D. Baró, F. Plazaola, and F. Baudelet: *Phys. Rev. B*, 2006, vol. 74, pp. 024407.
38. U. Admon, M.P. Dariel, E. Grunbaum, and J.C. Lodder: *J. Appl. Phys.*, 1987, vol. 62, p. 1943.
39. E. Pellicer, A. Varea, S. Pané, B.J. Nelson, E. Menéndez, M. Estrader, S. Surinach, M.D. Baró, J. Nogués, and J. Sort: *Adv. Funct. Mater.*, 2010, vol. 20, p. 983.
40. W.M. Daoush, K.H. Lee, H.S. Park *et al.*: *Int. J. Refract. Met. Hard Mater.*, 2009, vol. 27, pp. 83–89.
41. B. Nirmala, P.K. Vallal, R. Amuthan, and M. Mahendran: *Nanosci. Nanotechnol.*, 2011, vol. 1 (1), pp. 8–13.
42. F. Akhtar: *Int. J. Refract. Met. Hard Mater.*, 2008, vol. 26, pp. 145–51.
43. Y. Kim, K.H. Lee, E.P. Kim, D.I. Cheong, and S.H. Hong: *Int. J. Refract. Met. Hard Mater.*, 2009, vol. 27, pp. 842–46.